

Article citation info:

Huang Y, Zhang J, Wang B, Wei Y, An adaptive Kriging method focusing on reliability-sensitive space-time for time-variant reliability analysis, *Eksploracja i Niezawodność – Maintenance and Reliability* 2025; 27(4) <http://doi.org/10.17531/ein/203980>

An adaptive Kriging method focusing on reliability-sensitive space-time for time-variant reliability analysis

Indexed by:



Ying Huang^{a,b}, JianGuo Zhang^{a,b,*}, Bowei Wang^c, Yanxu Wei^d

^a School of Reliability and Systems Engineering, Beihang University, China

^b Hangzhou International Innovation Institute, Beihang University, China

^c School of Computer Science and Engineering, Beihang University, China

^d College of Mechanical and Vehicle Engineering, Taiyuan University of Technology, China

Highlights

- A new single loop Kriging method for time-variant reliability analysis is proposed.
- A reliability-sensitive region-based adaptive learning mechanism is designed.
- Four case studies illustrate the superiority of the proposed approach.
- This study clarifies the importance of focusing reliability-sensitive space-time region.

Abstract

The time-variant reliability analysis method based on the adaptive single-loop surrogate has attracted much attention due to its excellent computing performance. However, the existing methods do not sufficiently focus surrogate learning on the reliability-sensitive space-time region with high efficacy in improving the reliability surrogate, resulting in calculating waste. In this paper, a reliability-sensitive space-time Kriging (RSTK) modeling approach is proposed. In the RSTK, to screen out reliability-sensitive trajectory segments, a reliability-sensitive space-time determination method is first proposed; further, to capture high-quality training samples, a reliability-sensitive space-time learning approach is designed correspondingly; finally, a matching iteration termination criterion is constructed. Four case studies demonstrate the superiority of the proposed RSTK in reducing calculational costs. RSTK shortens the iteration time by one to two orders of magnitude and reduces the surrogate cost by up to 22.3% while maintaining accuracy.

Keywords

time-variant reliability analysis; adaptive Kriging modeling; single loop; reliability-sensitive space-time region

This is an open access article under the CC BY license (<https://creativecommons.org/licenses/by/4.0/>)

1. Introduction

For decades, time-invariant reliability analysis methods have been developed rapidly 1,. Neural network methods with strong data processing ability were employed to handle complex engineering problems 3,, and high-performance reliability modeling strategies and surrogate methods were designed 5,, which effectively improve the computing efficacy of time-invariant reliability analysis 7. Furthermore, the active learning surrogate modeling methods with high computing performance

(*) Corresponding author.

E-mail addresses:

Y. Huang (ORCID: 0000-0002-9524-6980) bhhuangying@buaa.edu.cn, J. Zhang (ORCID: 0009-0005-6692-8930) mech_reL619@buaa.edu.cn, B. Wang (ORCID: 0009-0001-9133-0472) wangboy0716@163.com, Y. Wei (ORCID: 0000-0001-9293-3649) weiyanyxu2013@163.com

and the reliability design methods incorporating active learning were proposed 8-. However, they ignore more general time-variant uncertainties (such as dynamic loads, material degradation, and aging) in practical engineering problems, which results in the distortion of analysis results 11,. In recent years, time-variant reliability analysis (TRA) has gained much attention, and it can assess the reliability of the research object over a period 13,. Due to random processes and time-variant

inputs, the computational load of each interest space point changes from time-invariant one-time calculation to multiple calculations of the time-variant trajectory, which considerably increases the calculating burden 15,. To alleviate the computing burden, numerous TRA approaches have been proposed, which can be divided into three categories: the outcrossing rate-based method, the composite limit state method, and the extremum surrogate-based method.

The outcrossing rate-based method estimates the failure probability by calculating the probability that the response trajectory crosses the allowable boundary, where different outcross events are assumed to be independent of each other 17. The efficient PHI2 method was proposed by integrating the first-order reliability method and the parallel static reliability model 18. To ensure the calculating stability of the PHI2 method, the PHI2+ approach was further developed 19. To expand the outcrossing rate-based method into scenarios with strongly correlated outcrossing events, the joint outcrossing rate method was designed 20. Despite the noticeable progress made 21,, the heavy response computing burden and assessment assumption still hinder their application in sophisticated engineering issues.

The composite limit state method discretizes the comprehensive failure problem in the full-time domain into a series of failure subproblems in sub-time domains. The TRPD method discretizes stochastic processes into random variables and then employs the first-order reliability method (FORM) to calculate the failure probability 23. Furthermore, to simplify the discretization analysis process and improve the efficiency of TRPD, the improved TRPD method was developed by designing a more efficient time-invariant transformation approach 24. To improve the calculating precision, the NEWREL method formulates the time-variant estimation as the large-scale series time-invariant evaluation 25. To elevate computing efficiency, the semi-analytical extreme value method was proposed by integrating the calculating advantages of the discrete method, the extremum method, and the Taylor series expansion approximation 26. Although appreciable advancements have been achieved 27,, these methods require vast actual response assessments, and the FORM or second-order reliability methods they employ struggle to achieve satisfactory accuracy in highly nonlinear problems.

To better balance accuracy and efficiency, the extremum

surrogate-based approach uses a low-cost surrogate model to characterize response trajectories and then performs the time-variant failure evaluation according to failure situations of the trajectory extremum. Building upon classical surrogate models (such as Kriging 29, artificial neural network 30, and support vector machine 31), the extremum surrogate methods have been proposed, such as the extremum response surface 32, extremum support vector machine 33, and extremum Kriging 34. This study focuses on the Kriging surrogate model due to its superior approximation performance, particularly its unique capability to evaluate prediction errors 35,, which can effectively guide the design of adaptive learning processes. Furthermore, a series of high-performance adaptive Kriging extremum methods have been developed by organically integrating the extremum Kriging method with the adaptive surrogate modeling approach. Wang et al. proposed a double-loop Kriging-based nested extreme response surface approach for TRA, in which the inner and outer loops are employed to identify extremum locations and calculate extremum responses, respectively 37. To improve the double-loop calculating efficiency, Hu et al. proposed a mixed efficient global optimization method 38. Furthermore, to avoid the time-consuming inner loop optimization, Wang et al. designed an equivalent stochastic process transformation (eSPT) approach 39; then, Hu et al. proposed a more general adaptive Kriging Monte Carlo-based single-loop Kriging (SILK) surrogate method 40,. Based on the SILK, to further improve TRA computing efficacy, Jiang et al. designed a real-time estimation error-guided active learning method (REAL), in which the derived real-time errors are used to acquire high-quality surrogate samples 42. Gao et al. proposed a SILK based on the candidate sample pool reduction strategy (SLK-CSPR), which improves computational efficiency by controlling the iterative computation burden 43. Tian et al. proposed a stratified sampling-based time-variant Kriging modeling approach (SSTK), which guarantees computational efficacy by using the designed learning function to capture training data in different spatial layers 44. Several other works are also noteworthy 45-. These single-loop adaptive learning surrogate methods effectively ensure the reliability analysis efficacy for time-variant problems. However, most existing methods determine the high-quality surrogate samples by comprehensively considering the full-time-domain sample information of

candidate trajectories; this adaptive learning design, which does not exclude the regions that have already been accurately identified, fails to adequately focus the surrogate description on reliability-sensitive regions, resulting in a waste of surrogate modeling cost and iterative computing time. A large prediction error of the response trajectory far away from the limit state may not affect the correctness of trajectory failure classification, thus, the surrogate modeling for TRA should sufficiently focus on the reliability-sensitive space-time regions near the limit state.

To address the above issues, a reliability-sensitive space-time Kriging (RSTK) approach is proposed in this study. By determining whether the distribution range of the predicted response crosses the limit state, a reliability-sensitive recognition formula is proposed; further, by comprehensively considering the surrogate credibility level and series failure traits of the reliability-sensitive trajectory segments, the reliability-sensitive learning method is designed; finally, the corresponding stopping criterion is established. Unlike existing adaptive learning designs based on full-time-domain trajectory information, the proposed RSTK can effectively focus the surrogate representation on reliability-sensitive regions by excluding non-reliability-sensitive information during surrogate sample selection and performing the corresponding adaptive learning; this facilitates the acquisition of high-quality training data and avoids the iterative computation of numerous candidate samples. The proposed method is verified using four cases. The main contribution of this study is the proposal of the adaptive TRA concept that adequately focuses on the reliability-sensitive space-time and to clarify its importance for time-variant reliability surrogate representation.

The rest of this paper: Section 2 briefly describes the Kriging extremum surrogate-based TRA background; Section 3 introduces the proposed method; Section 4 validates the superiority of the proposed method; Section 5 presents the conclusions and outlooks.

2. Fundamental background

2.1. Time-variant reliability analysis

In the time-variant reliability analysis, a stochastic response process is judged to fail when a failure moment exists, and the time-variant failure probability is calculated as follows:

$$P_f(t_0, t_e) = P_r\{g(\mathbf{X}, \mathbf{Y}(t), t) \leq 0, \exists t \in [t_0, t_e]\} \quad (1)$$

where, $P_r\{\cdot\}$ represents the probability operator; $g(\mathbf{X}, \mathbf{Y}(t), t)$ is the limit state response at the time node t ; $[t_0, t_e]$ is the time interval; $\mathbf{X} = [X_1, X_2, \dots, X_{nx}]$ is the random vector with nx variables; $\mathbf{Y}(t) = [Y_1(t), Y_2(t), \dots, Y_{ny}(t)]$ is the stochastic process vector with ny stochastic processes.

In the stochastic process expression, $Y(t)$ can be represented using a series of standard normal variables $\xi = (\xi_1, \xi_2, \dots, \xi_D)$ after performing EOLE (i.e., expansion optimal linear estimation) 49, as follows:

$$Y(t) = \mu_Y(t) + \sigma_Y(t) \sum_{i=1}^D \frac{\xi_i}{\sqrt{\lambda_i}} \Phi_i \mathbf{C}(t) \quad (2)$$

where, $\mu_Y(t)$ and $\sigma_Y(t)$ are the mean function and the standard deviation function of $Y(t)$, respectively; D is the number of dominated eigenvalues; λ_i and Φ_i are the eigenvalue and eigenvector of the correlation matrix \mathbf{C} ($C_{ij} = \rho(t_{i1}, t_{ij})$, $t_i, t_j = 1, 2, \dots, Nt$), respectively; $\rho(t_{i1}, t_{ij})$ is the autocorrelation function of $Y(t)$; Nt is the number of time nodes.

Based on the Monte Carlo (MC) method and the extreme value failure principle 50, the time-variant failure probability is further expressed as Eq. (3) and its schematic diagram is depicted in Figure 1.

$$P_f(t_0, t_e) = \frac{\sum_{j=1}^{Nm} I_{\min}(X^j, (\xi_1, \xi_2, \dots, \xi_{ny}), t)}{Nm} \quad (3)$$

where, Nm is the MC samples number; $I_{\min}(X^j, (\xi_1, \xi_2, \dots, \xi_{ny}))$ is the time-variant failure indicator function and its expression is:

$$I_{\min}(X^j, (\xi_1, \xi_2, \dots, \xi_{ny}), t) = \begin{cases} 1 & \min_{t_i=1, 2, \dots, Nt} g(X^j, (\xi_1, \xi_2, \dots, \xi_{ny}), t_i) \leq 0 \\ 0 & \min_{t_i=1, 2, \dots, Nt} g(X^j, (\xi_1, \xi_2, \dots, \xi_{ny}), t_i) > 0 \end{cases} \quad (4)$$

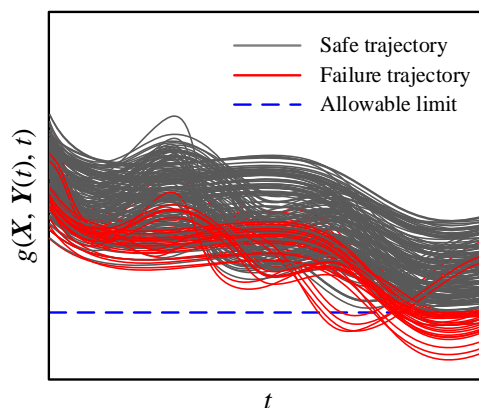


Figure 1. Schematic diagram of the time-variant reliability calculation

2.2. Kriging-based extremum method

Kriging model can be described as 51:

$$y(\mathbf{x}) = \mathbf{f}(\mathbf{x})^T \boldsymbol{\beta} + z(\mathbf{x}) \quad (5)$$

where, $\mathbf{f}(\mathbf{x}) = [f_1(\mathbf{x}), f_2(\mathbf{x}), \dots, f_p(\mathbf{x})]^T$ is the regression basis function; $\boldsymbol{\beta} = [\beta_1, \beta_2, \dots, \beta_p]^T$ is the regression coefficient vector; stochastic process $z(\mathbf{x})$ obeys the Gaussian distribution $N(0, \sigma^2)$, and its covariance is:

$$\text{Cov}[z(\mathbf{x}_u), z(\mathbf{x}_v)] = \sigma^2 R(\mathbf{x}_u, \mathbf{x}_v; \boldsymbol{\theta})$$

$$\text{s.t. } R(\mathbf{x}_u, \mathbf{x}_v; \boldsymbol{\theta}) = \prod_{i=1}^m \exp[-\theta_i(x_{ui} - x_{vi})^2] \quad (6)$$

where, \mathbf{x}_u and \mathbf{x}_v represent two random inputs; σ^2 is the process variance; $\boldsymbol{\theta}$ is the Kriging parameter vector; $R(\cdot)$ is the Gaussian correlation function; m is the input dimension; θ_i is the i -th member of $\boldsymbol{\theta}$.

Further, the optimal Kriging parameter $\boldsymbol{\theta}'$ can be solved using the maximum likelihood estimation, as follows:

$$\boldsymbol{\theta}' = \text{argmin}\{\varphi(\boldsymbol{\theta})\} = \text{argmin}\{\sigma^2 |\mathbf{R}|^{1/n}\} \quad (7)$$

where, \mathbf{R} is the correlation matrix; n is the training samples number.

Upon acquisition of the optimal parameter $\boldsymbol{\theta}'$, the corresponding regression coefficient $\boldsymbol{\beta}'$ and process variance σ'^2 are correspondingly determined as follows:

$$\begin{cases} \boldsymbol{\beta}' = (\mathbf{f}(\mathbf{x})^T \mathbf{R}'^{-1} \mathbf{f}(\mathbf{x}))^{-1} \mathbf{f}(\mathbf{x})^T \mathbf{R}' \mathbf{y} \\ \sigma'^2 = \frac{1}{n} (\mathbf{y} - \mathbf{f}(\mathbf{x}) \boldsymbol{\beta}')^T \mathbf{R}'^{-1} (\mathbf{y} - \mathbf{f}(\mathbf{x}) \boldsymbol{\beta}') \end{cases} \quad (8)$$

where \mathbf{R}' is the correlation matrix corresponding to $\boldsymbol{\theta}'$; \mathbf{y} is the outputs corresponding to n training inputs $\mathbf{x} = [\mathbf{x}_1, \mathbf{x}_2, \dots, \mathbf{x}_n]$. Further, the mean value $\mu_{\hat{g}}(\mathbf{x}_a)$ and variance $\sigma_{\hat{g}}^2(\mathbf{x}_a)$ of the Kriging prediction to an interested point \mathbf{x}_a can be computed as:

$$\begin{aligned} \mu_{\hat{g}}(\mathbf{x}_a) &= \mathbf{f}^T(\mathbf{x}_a) \boldsymbol{\beta}' + \mathbf{r}^T(\mathbf{x}_a) \mathbf{R}'^{-1} (\mathbf{y} - \mathbf{f}(\mathbf{x}) \boldsymbol{\beta}') \\ \sigma_{\hat{g}}^2(\mathbf{x}_a) &= \sigma'^2 \{1 + \mathbf{u}^T(\mathbf{x}_a) [(\mathbf{f}(\mathbf{x})^T \mathbf{R}'^{-1} \mathbf{f}(\mathbf{x}))^{-1} \mathbf{u}(\mathbf{x}) \\ &\quad - \mathbf{r}(\mathbf{x}_a)^T \mathbf{R}'^{-1} \mathbf{r}(\mathbf{x})]\} \\ \text{s.t. } \mathbf{u}(\mathbf{x}_a) &= \mathbf{f}(\mathbf{x})^T \mathbf{R}'^{-1} \mathbf{r}(\mathbf{x}_a) - \mathbf{f}(\mathbf{x}_a) \end{aligned} \quad (9)$$

where, $\mathbf{r}(\mathbf{x}_a) = [R(\mathbf{x}_a, \mathbf{x}_1; \boldsymbol{\theta}'), R(\mathbf{x}_a, \mathbf{x}_2; \boldsymbol{\theta}'), \dots, R(\mathbf{x}_a, \mathbf{x}_m; \boldsymbol{\theta}')]^T$ is the correlation vector.

From the preceding discussion, it can be observed that the Kriging prediction for any sample of interest $(\mathbf{X}, \mathbf{Y}(t), t)$ follows a normal distribution $N(\mu_{\hat{g}}(\cdot), \sigma_{\hat{g}}^2(\cdot))$, in which $\mu_{\hat{g}}(\cdot)$ is utilized for response prediction and $\sigma_{\hat{g}}^2(\cdot)$ is employed to guide adaptive learning [52]. Notably, for a time-variant problem with nx random variables, ny random processes, and a time variable, the Kriging inputs dimension

(i.e.,

$[\mathbf{X}, ((\xi_1, \xi_2, \dots, \xi_{D_1})_1, (\xi_1, \xi_2, \dots, \xi_{D_2})_2, \dots, (\xi_1, \xi_2, \dots, \xi_{D_{ny}})_{ny}), t]$
) is $nx + \sum_{i=1}^{ny} D_i + 1$, where D_i represents the number of standard normal random variables used for characterizing

stochastic processes, as showed in Eq. (2); furthermore, the D of some random processes is relatively high, while Kriging struggles to effectively characterize high-dimensional problems. To handle this problem, the random processes rather than expanded random variables are used as Kriging inputs in this study, which sharply decreases the Kriging surrogate dimension from $nx + \sum_{i=1}^{ny} D_i + 1$ to $nx + ny + 1$, as follows:

$$\begin{bmatrix} \mathbf{X}^{(1)} (\xi_1^{(1)}, \xi_2^{(1)}, \dots, \xi_i^{(1)}, \dots, \xi_{ny}^{(1)}) & t_{t_1} \\ \mathbf{X}^{(2)} (\xi_1^{(2)}, \xi_2^{(2)}, \dots, \xi_i^{(2)}, \dots, \xi_{ny}^{(2)}) & t_{t_2} \\ \vdots & \vdots \\ \mathbf{X}^{(n)} (\xi_1^{(n)}, \xi_2^{(n)}, \dots, \xi_i^{(n)}, \dots, \xi_{ny}^{(n)}) & t_{t_n} \end{bmatrix} \rightarrow \begin{bmatrix} \mathbf{X}^{(1)} & \mathbf{Y}^{(1)} & t_{t_1} \\ \mathbf{X}^{(2)} & \mathbf{Y}^{(2)} & t_{t_2} \\ \vdots & \vdots & \vdots \\ \mathbf{X}^{(n)} & \mathbf{Y}^{(n)} & t_{t_n} \end{bmatrix} \quad (10)$$

where, $\xi_i = (\xi_1, \xi_2, \dots, \xi_{D_i})_i$.

After Kriging modeling, the trained Kriging is employed to predict the responses $\mu_{\hat{g}}(\mathbf{X}, \mathbf{Y}(t), t)$ of MC samples, then the Kriging prediction-based time-variant failure probability is finally acquired by evaluating the trajectories extremum, as follows:

$$\hat{P}_f(t_0, t_e) = \frac{\sum_{j=1}^{Nm} I_{\min}(\mathbf{X}^j, (Y_1^j(t), Y_2^j(t), \dots, Y_{ny}^j(t)), t)}{Nm} \quad (11)$$

where, the failure indicator function $I_{\min}(\cdot)$ is expressed as follows:

$$I_{\min}(\mathbf{X}^j, (Y_1^j(t), Y_2^j(t), \dots, Y_{ny}^j(t)), t) = \begin{cases} 1 & \min_{t_i=1,2,\dots,Nt} \mu_{\hat{g}}(\mathbf{X}^j, (Y_1^j(t_i), Y_2^j(t_i), \dots, Y_{ny}^j(t_i)), t_i) \leq 0 \\ 0 & \min_{t_i=1,2,\dots,Nt} \mu_{\hat{g}}(\mathbf{X}^j, (Y_1^j(t_i), Y_2^j(t_i), \dots, Y_{ny}^j(t_i)), t_i) > 0 \end{cases} \quad (12)$$

3. Proposed method

3.1. Adaptive learning analysis for time-variant reliability

In time-variant reliability analysis, a large calculation error of a point in a non-sensitive segment (as shown in Figure 2 (a)) and a non-sensitive space sample in a time point (as shown in Figure 2 (b)) may not affect the reliability judgment, because their responses are far from the allowable limit. Indiscriminate full-space-time adaptive learning is prone to capturing excessive unimportant non-sensitive space-time information, which poorly contributes to reliability surrogate enhancement, leading to significant computational waste.

Essentially, adaptive learning of TRA involves information screening across the space and time dimensions and encompasses three adaptive learning strategies; strategy 1: determining the space point first, then the time point; strategy 2: determining the time point first, then the space point; strategy 3: simultaneously determining the space point and time point. It

should be noted that in the full-time and full-space domains of adaptive reliability analysis, there are numerous space points and moments/periods whose failure conditions have been accurately evaluated, especially in the later stages of adaptive iterations. These space-time locations contribute minimally, or even ineffectively, to improving reliability surrogates, and adaptive learning that comprehensively considers such redundant information significantly hinders the efficient acquisition of high-quality time-variant samples. Specifically, strategy 1 needs to comprehensively consider the surrogate information of space points in the full-time domain. It may focus on the space points that have accurately performed the reliability classification, as the candidate trajectories with large full-time surrogate errors might already have been accurately judged as failure at certain moments. Figure 3 (a) illustrates the trajectory prediction for the time-variant problem $g(x_1, x_2, t) = x_1^2 - 2tx_2^2 - t^2 + 28$ at the location (1.8, 2.3), which may raise concern in the iterations due to its large prediction error, but which has accurately judged reliability since it is accurately determined to be a failure at time t_0 . Similarly, strategy 2 requires a comprehensive consideration of the surrogate

information of all space points at the time point of interest. It unavoidably focuses on the sub-time domains with high analysis accuracy, as some sub-time domains may exhibit satisfactory reliability analysis accuracy despite having large full-space surrogate errors. Figure 3 (b) shows the space prediction of $g(x_1, x_2, t) = x_1^2 - 2tx_2^2 - t^2 + 28$ at $t = 2.5$, which may raise concern due to its large total prediction error, but accurate reliability classification has been achieved, as the large errors of these space points do not affect their reliability judgment. Strategy 3 needs to comprehensively consider all space-time surrogate information, and it may encounter similar issues faced by strategies 1 and 2. Therefore, in adaptive learning for TRA, the comprehensive consideration of space-time information, without excluding redundant data, will inevitably focus on the space-time data that have limited or even negligible impact on reliability surrogate, which significantly hinders the capture of high-quality time-variant data in adaptive surrogate modeling. Implementing surrogate modeling that can fully focus on reliability-sensitive space-time is of great significance in improving TRA calculating efficacy.

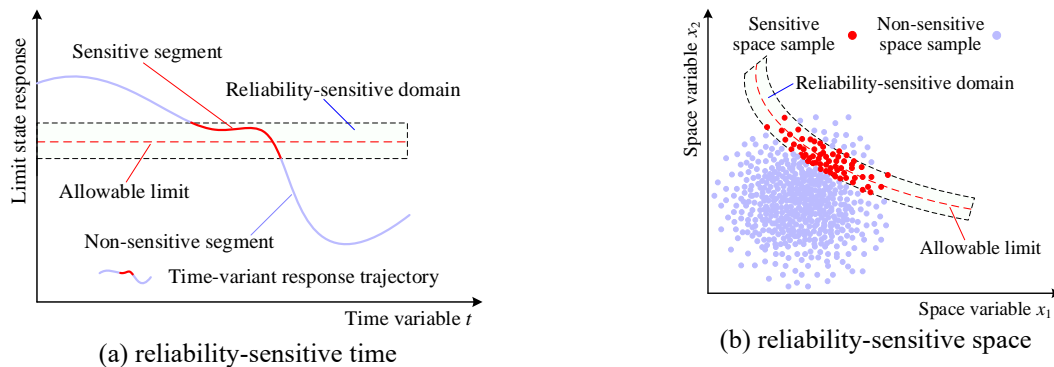


Figure 2. Schematic diagram of the proposed reliability-sensitive space-time.

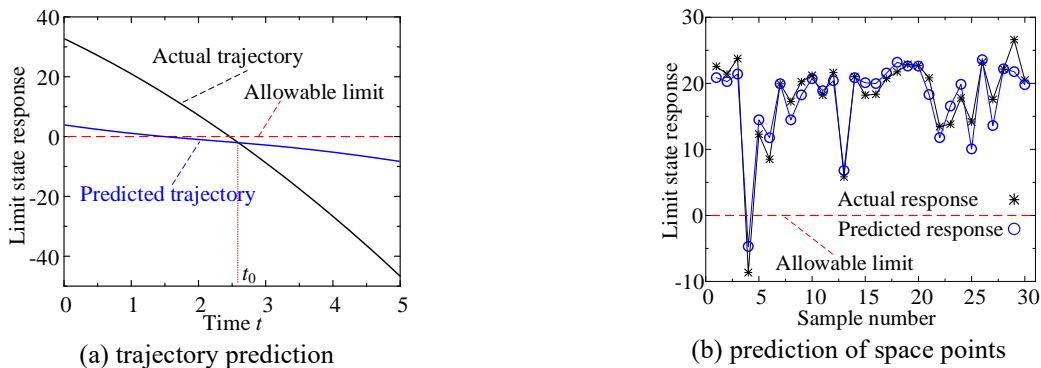


Figure 3. Diagram of trajectory and space position prediction.

3.2. Determination of reliability-sensitive space-time

Reliability-sensitive space-time refers to the region near the

limit state where the time-variant reliability indicator is easily misjudged. It is challenging to determine appropriate reliability-

sensitive space-time segments due to frequent obstacles in obtaining required relevant information, such as response gradients and response magnitudes. To address this challenge, a prediction distribution information-based reliability-sensitive space-time recognition thought is proposed: the region where the upper and lower bounds of the Kriging prediction-based normal distribution can cross over the limit state is regarded as the reliability-sensitive space-time and the designing thought is schematically illustrated in Figure 4. Furthermore, the corresponding sensitive sample capture formula is proposed as Eq. (13). Eq. (13) is utilized to exclude non-reliability-sensitive samples in active learning; this design, which avoids focusing on low-quality samples, holds the potential to improve the reliability analysis efficacy. This approach can effectively identify the reliability-sensitive region because the upper and lower limits of the prediction distribution intersect with the limit state, indicating that the predicted sample has a prediction response close to the allowable limit and a large prediction fluctuation. These are precisely the reliability-sensitive samples requiring attention in reliability surrogate modeling. The Eq. (13)-based reliability-sensitive screening operation is capable of considering both the prediction error and the difference between the predicted value and the allowable limit, and adaptively

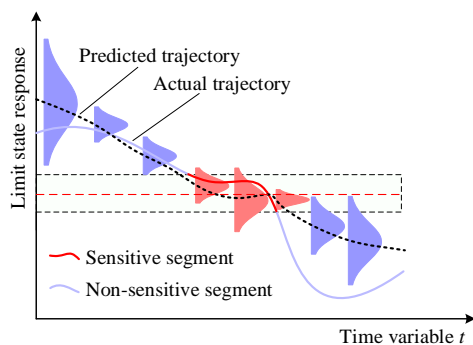
adjusting the reliability-sensitive samples of concern as surrogate accuracy iteratively improves. This dynamic multi-consideration-based reliability-sensitive recognition has the potential to constrain the adaptive learning to reliability surrogate samples with low boosting.

$$\mathcal{S}_s = \{(\mathbf{X}, \mathbf{Y}(t), t) \in$$

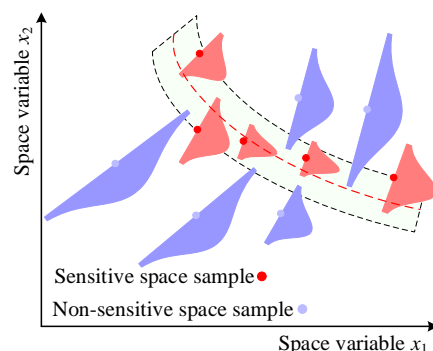
$$\mathcal{S}_{mc} | F^{-1}\left(\frac{1-p}{2}, \mu_{\hat{g}}(\mathbf{X}, \mathbf{Y}(t), t), \sigma_{\hat{g}}(\mathbf{X}, \mathbf{Y}(t), t)\right) \cdot$$

$$F^{-1}\left(\frac{1+p}{2}, \mu_{\hat{g}}(\mathbf{X}, \mathbf{Y}(t), t), \sigma_{\hat{g}}(\mathbf{X}, \mathbf{Y}(t), t)\right) \leq 0\} \quad (13)$$

where, \mathcal{S}_s is the reliability-sensitive samples; \mathcal{S}_{mc} is the candidate samples; $F^{-1}(\cdot)$ is the inverse function of the normal cumulative distribution function; $F^{-1}((1-p)/2, \mu_{\hat{g}}(\cdot), \sigma_{\hat{g}}(\cdot))$ is the input corresponding to the normal distribution with the Kriging mean $\mu_{\hat{g}}(\cdot)$ and Kriging standard deviation $\sigma_{\hat{g}}(\cdot)$ at the cumulative probability $(1-p)/2$. p is the information coverage percentage of prediction distribution, as illustrated in Figure 5. Given that a larger p -value indicates more samples identified as reliability-sensitive during the iteration and higher calculating accuracy, this study sets $p = 99.5\%$ to ensure computing accuracy.



(a) reliability-sensitive time



(b) reliability-sensitive space

Figure 4. Thought of the reliability-sensitive space-time identification based on the prediction distribution information.

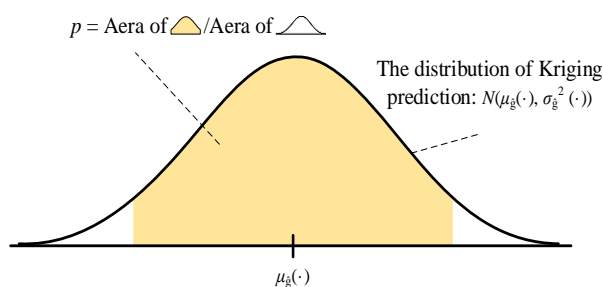


Figure 5. Schematic diagram of the value of parameter p .

3.3. Reliability-sensitive space-time learning

Adaptive learning based on the non-reliability-sensitive space-time with a high correct classification probability is inefficient or even ineffective in improving the reliability surrogate efficacy. Therefore, to efficiently acquire high-quality reliability surrogate data, a reliability-sensitive space-time learning approach is proposed by organically integrating the time-variant failure traits and credibility of reliability-sensitive trajectory segments.

The Kriging prediction follows a normal distribution $N(\mu_{\hat{g}}(\cdot), \sigma_{\hat{g}}^2(\cdot))$. For any sample of interest $(\mathbf{X}, \mathbf{Y}(t), t)$, if the predicted response $\mu_{\hat{g}}(\mathbf{X}, \mathbf{Y}(t), t) > 0$, then the correct classification probability of reliability sign is the probability of obtaining a variable exceeding 0 in a normal distribution, as shown in Eq. (14). Conversely, if $\mu_{\hat{g}}(\mathbf{X}, \mathbf{Y}(t), t) < 0$, it is the probability of capturing a variable being below 0 in a normal distribution, as shown in Eq. (15). Figure 6 illustrates these two situations.

$$P_p = 1 - \Phi\left(\frac{(0 - \mu_{\hat{g}}(\mathbf{X}, \mathbf{Y}(t), t))}{\sigma_{\hat{g}}(\mathbf{X}, \mathbf{Y}(t), t)}\right) \quad (14)$$

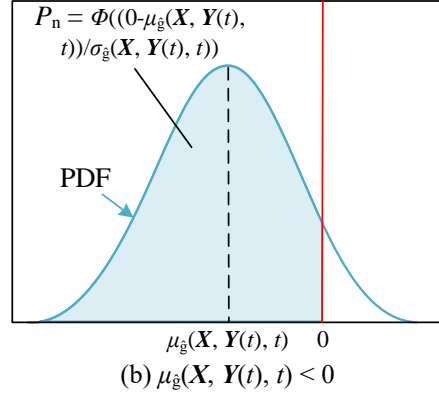
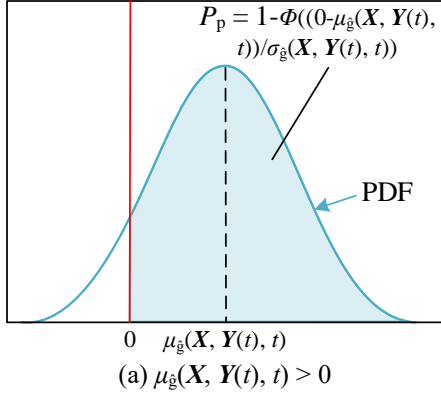


Figure 6. The correct classification probability of Kriging prediction.

Considering the series failure characteristics (failure at any moment causes the trajectory to fail) in the reliability judgment of response trajectory, the trajectories with $\mu_{\hat{g}}(\cdot) \leq 0$ and $U(\cdot) \geq 2$ are considered as the non-reliability-sensitive trajectories ($U(\cdot) \geq 2$ means at least $\Phi(2) = 99.73\%$ correct probability of reliability judgment 41). Similarly, the trajectories with $\mu_{\hat{g}}(\cdot) \leq 0$ in the non-sensitive space-time, as well as the trajectories entirely within the non-sensitive region are also regarded as non-reliability-sensitive trajectories. All other trajectories are considered reliability-sensitive trajectories. To effectively eliminate the influence of redundant non-sensitive information,

$$L_X(\mathbf{X}^i) = \begin{cases} \text{IC, if } \mu_{\hat{g}}(\mathbf{X}^i, \mathbf{Y}^i(t^j), t^j) \leq 0 \text{ and } U(\mathbf{X}^i, \mathbf{Y}^i(t^j), t^j) \geq 2, \exists j = 1, 2, \dots, Nt \\ \text{IC, if } \mu_{\hat{g}}(\mathbf{X}^i, \mathbf{Y}^i(t^j), t^j) \leq 0 \text{ and } (\mathbf{X}^i, \mathbf{Y}^i(t^j), t^j) \notin \mathcal{S}_s, \exists j = 1, 2, \dots, Nt \\ ACL^i, \text{ otherwise} \end{cases} \quad (17)$$

where, IC is an infinite constant; ACL^i is the reliability-sensitive confidence level of space sample \mathbf{X}^i , as follows:

$$ACL^i = \frac{\sum_{j=1}^{Nt} I_e(\mathbf{X}^i, \mathbf{Y}^i(t^j), t^j) P_e(\mathbf{X}^i, \mathbf{Y}^i(t^j), t^j)}{\sum_{j=1}^{Nt} I_e(\mathbf{X}^i, \mathbf{Y}^i(t^j), t^j)} \quad (18)$$

where, $P_e(\cdot)$ is the correct classification probability calculated using Eq. (16); $I_e(\mathbf{X}^i, \mathbf{Y}^i(t^j), t^j)$ is the reliability-sensitive indicator function and its expression is:

$$P_n = \Phi\left(\frac{(0 - \mu_{\hat{g}}(\mathbf{X}, \mathbf{Y}(t), t))}{\sigma_{\hat{g}}(\mathbf{X}, \mathbf{Y}(t), t)}\right) \quad (15)$$

where, $\Phi(\cdot)$ is the cumulative distribution function of the standard normal. Thus, whether $\mu_{\hat{g}}(\mathbf{X}, \mathbf{Y}(t), t) > 0$ or $\mu_{\hat{g}}(\mathbf{X}, \mathbf{Y}(t), t) < 0$, the correct classification probability of the $\mu_{\hat{g}}(\mathbf{X}, \mathbf{Y}(t), t)$ sign can be formulated as:

$$P_e = \Phi(U) \quad (16)$$

where, $U = |\mu_{\hat{g}}(\mathbf{X}, \mathbf{Y}(t), t)| / \sigma_{\hat{g}}(\mathbf{X}, \mathbf{Y}(t), t)$.

the adaptive learning of RSTK focuses exclusively on the sensitive segments of reliability-sensitive trajectories. Furthermore, given that the sensitive segments of various trajectories have different lengths, and the learning operation simultaneously considering predicted information of multiple sensitive moments facilitates improving the overall reliability-sensitive surrogate effect, a reliability-sensitive confidence is designed to assure the enhancement efficacy of reliability-sensitive description in each learning. The reliability-sensitive space-time learning function is finally designed as:

$$I_e(\mathbf{X}^i, \mathbf{Y}^i(t^j), t^j) = \begin{cases} 1 & (\mathbf{X}^i, \mathbf{Y}^i(t^j), t^j) \in \mathcal{S}_s \\ 0 & (\mathbf{X}^i, \mathbf{Y}^i(t^j), t^j) \notin \mathcal{S}_s \end{cases} \quad (19)$$

For the reliability-sensitive trajectories, the space position $(\mathbf{X}^m, \mathbf{Y}^m)$ with the minimum $L_X(\cdot)$ is first identified, as follows:

$$(\mathbf{X}^m, \mathbf{Y}^m) = \underset{i=1, 2, \dots, Nn}{\operatorname{argmin}} \{L_X(\mathbf{X}^i)\} \quad (20)$$

where, Nn is the number of reliability-sensitive trajectories ($Nn < Nm$), i.e., the number of the samples that satisfy $L_X(\mathbf{X}) \neq \text{IC}$.

Then, the new sample \mathcal{S}_{add} is determined as follows:

$$\mathcal{S}_{\text{add}} = (\mathbf{X}^m, \mathbf{Y}^m(t^n), t^n)$$

$$(\mathbf{Y}^m(t^n), t^n) = \operatorname{argmin} U(\mathbf{X}^m, \mathbf{Y}^m(t^j), t^j), j = 1, 2, \dots, Nt_m \quad (21)$$

where, Nt_m is the number of sensitive moments in the trajectory corresponding to the space sample \mathbf{X}^m ($Nt_m < Nt$).

In each adaptive iteration, Eq. (20) is used to identify the trajectory of interest ($\mathbf{X}^m, \mathbf{Y}^m$) corresponding to the new sample from the reliability-sensitive trajectories screened using Eq. (17); then, Eq. (21) is applied to extract the time point of interest in ($\mathbf{X}^m, \mathbf{Y}^m$) to determine the new modeling sample.

Additionally, to avoid the issue of sample aggregation, the new sample is required to satisfy the space correlation constraint, as follows:

$$\max_{i=1,2,\dots,Ne} \{ \operatorname{corr}(\mathcal{S}_{\text{add}}, \mathcal{S}_i) \} < \varepsilon_{\text{corr}} \quad (22)$$

where, Ne is the number of existing training samples; $\varepsilon_{\text{corr}}$ is the Kriging space correlation threshold, and is set as 0.99 in this study 40. In detail, Eq. (22) is first employed to calculate the correlation metric corr between candidate samples and the current training set; then, by ignoring the candidate samples

satisfying $\operatorname{corr} \geq 0.99$ during the modeling sample identification process, sample clustering is avoided.

Notably, the designed reliability-sensitive space-time learning method only requires calculating the reliability-sensitive space-time positions of the reliability-sensitive trajectories in each iteration, and can adaptively adjust the focused sensitive segments based on the evolution of surrogate precision. The candidate computing burden of each iteration gradually decreases as the iteration progresses, as demonstrated in Figure 7. This adaptive learning design, which focuses on reliability-sensitive space-time, suppresses the iterative calculations and surrogate learning for the non-reliability-sensitive space-time regions with low reliability-elevating effects, which can productively reduce the surrogate modeling cost and iterative calculation time while ensuring computing precision. Moreover, the reliability-sensitive space-time credibility information is organically combined with the trajectory series failure characteristics in the designed adaptive learning, further ensuring the surrogate improvement efficacy of each sensitive learning iteration.

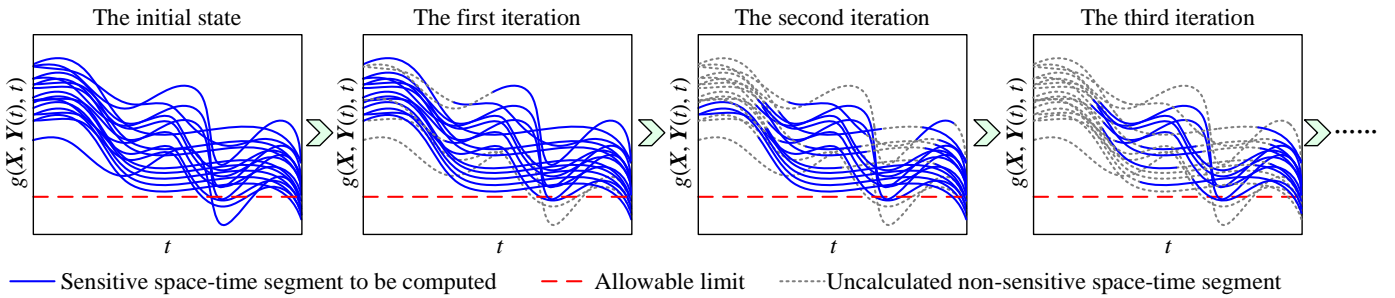


Figure 7. Schematic diagram of the iterative cost reduction effect of the proposed method.

3.4. Stopping criterion

As the iteration progresses, the failure probability evaluation error decreases progressively, and the number of non-reliability-sensitive trajectories gradually diminishes. Based on these features, a convergence criterion that synergistically considers both iterative trends is designed. From the perspective of reliability-sensitive surrogate identification, the proportion of non-reliability-sensitive trajectories is employed to evaluate the reliability surrogate accuracy of the entire space-time, as follows:

$$C = \frac{\sum_{i=1}^{Nm} I_c(\mathbf{X}^i)}{Nm} \quad (23)$$

where, $I_c(\mathbf{X}^i)$ is the indicator function of reliability-sensitive

trajectory, as shown in Eq. (24). The Kriging is considered well-trained if $C > 99.9\%$. Combining with Eq. (17), if all non-reliability-sensitive trajectories are determined based on $U(\mathbf{X}^i, \mathbf{Y}^i(t^j), t^j) > 2$, then $C > 99.9\%$ implies that at least $99.9\% \times \Phi(2) = 97.63\%$ of the trajectories are accurately classified; similarly, combining with Eq. (13) and Figure 5, if all non-reliability-sensitive trajectories are determined based on $(\mathbf{X}^i, \mathbf{Y}^i(t^j), t^j) \notin \mathcal{S}_s$, then $C > 99.9\%$ implies that at least $99.9\% \times [1 - (1-p)/2] = 99.65\%$ of the trajectories are accurately classified.

$$I_c(\mathbf{X}^i) = \begin{cases} 1 & L_X(\mathbf{X}^i) = \text{IC} \\ 0 & \text{otherwise} \end{cases} \quad (24)$$

From the perspective of the failure probability estimation accuracy, the $P_{\text{f}}(t_0, t_c)$ evaluation error er based on the current Kriging surrogate can be described as:

$$er = \frac{|\hat{P}_f(t_0, t_e) - P_f^*(t_0, t_e)|}{P_f^*(t_0, t_e)} = \frac{|N_{f2} - N_{f2}^*|}{N_{f1} + N_{f2}^*} \quad (25)$$

where, $\hat{P}_f(\cdot)$ is the predicted failure probability; $P_f^*(\cdot)$ is the actual failure probability; N_{f1} and N_{f2} are the predicted number of failure trajectories in non-reliability-sensitive and reliability-sensitive candidate trajectories, respectively, and are calculated using Eq. (26) and Eq. (27); N_{f2}^* is the actual trajectories number corresponding to N_{f2} . When $P_f^*(t_0, t_e) = 0$, er is set as a constant greater than 1 to satisfy the condition for continuing the iterative calculations.

$$N_{f1} = \sum I_{ic}; I_{ic} = \begin{cases} 1 & L_X(\mathbf{X}) = IC \text{ and } \mu_{\hat{g}}(\mathbf{X}, \mathbf{Y}(t^j), t^j) \leq 0 \quad \exists j = 1, 2, \dots, Nt \\ 0 & \text{otherwise} \end{cases} \quad (26)$$

$$N_{f2} = \sum I_{nic}; I_{nic} = \begin{cases} 1 & L_X(\mathbf{X}) \neq IC \text{ and } \mu_{\hat{g}}(\mathbf{X}, \mathbf{Y}(t^j), t^j) \leq 0 \quad \exists j = 1, 2, \dots, Nt \\ 0 & \text{otherwise} \end{cases} \quad (27)$$

Denote N_2 as the total number of the reliability-sensitive candidate trajectories, then we have $0 \leq N_{f2}^* \leq N_2$. Furthermore, the maximum er_{\max} of er , i.e., the maximum possible error of the estimated time-variant failure probability, can be derived as:

$$er_{\max} = \max_{N_{f2}^* \in [0, N_2]} \frac{|N_{f2} - N_{f2}^*|}{N_{f1} + N_{f2}^*} \quad (28)$$

The Kriging is considered well-trained if $er_{\max} < 5\%$.

The adaptive learning process is terminated when $C > 99.9\%$ or $er_{\max} < 5\%$ is satisfied. This iterative termination design, which synergistically considers failure evaluation accuracy and reliability-sensitive traits, helps to avoid redundant learning.

3.5. Implementation procedure of proposed approach

According to the contents in subsections 0-0, the core implementation process of RSTK is summarized as: the current Kriging is used to identify the non-reliability-sensitive trajectories and the non-reliability-sensitive space-time trajectory segments, and then high-quality modeling data is recognized in reliability-sensitive space-time segments to refine Kriging. These steps are repeated until the termination condition is triggered, and the reliability analysis is finally performed, as shown in Figure 8. The corresponding detailed steps are given in Figure 9.

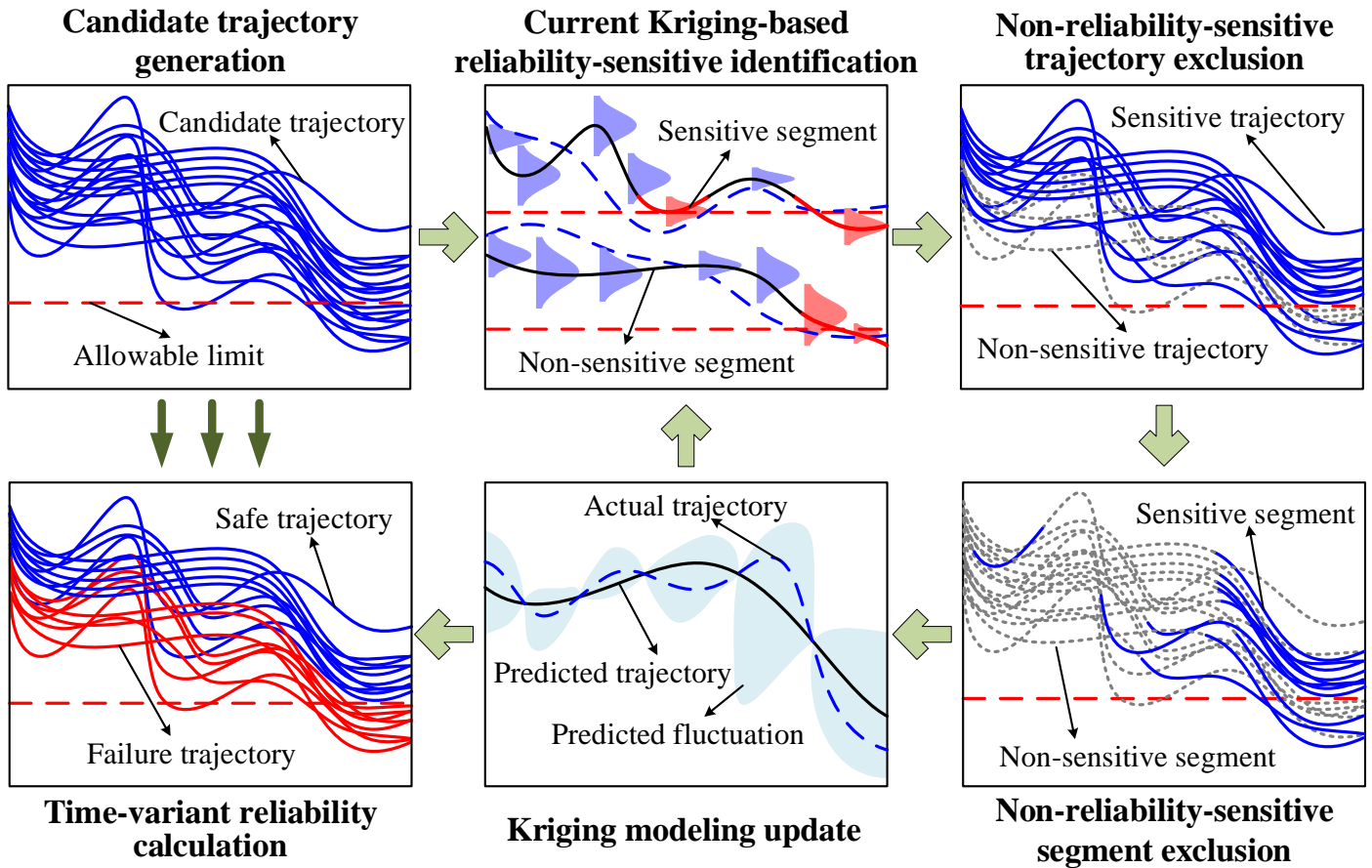


Figure 8. Schematic of the proposed approach-based adaptive surrogate.

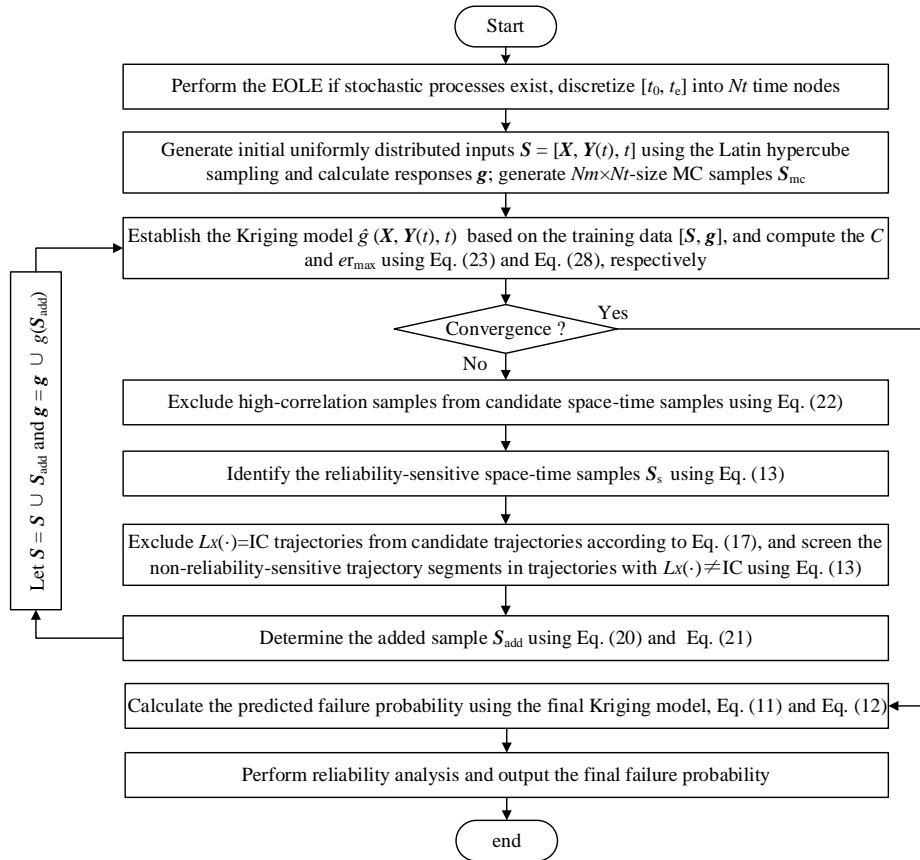


Figure 9. Flow of reliability analysis based on the proposed method.

4. Case studies

In this section, three numerical cases and one engineering case are employed to demonstrate the superior efficiency and accuracy of the proposed RSTK, in which the representative methods are used as comparison methods, including eSPT 39, SILK 40, REAL 42, SLK-CSPR 43, and SSTK 44. Their convergence criteria are set as cumulative conformance level $CCL > 99.999\%$, maximum percentage error $MPE < 5\%$, maximum real-time estimation error $MREE < 5\%$, minimum learning function $Ux > 2$, and minimum learning function $IAU > 1$, respectively. The MC result is seen as the “true” value. The call times N_{call} of actual response and CPU computing time of adaptive iteration are utilized as the efficiency metric, and the relative error (as formulated in Eq. (29)) is employed as the precision metric. In each case, N_{call} is determined based on the adaptive learning method and stopping criteria of each approach; in each call, new samples are processed using the actual response model to obtain outputs for updating the modeling data. All computations are performed using a Laptop Computer (AMD Ryzen 7 5800H CPU, 3.20 GHz, and 16 GB RAM). To ensure the comparability of results from different methods, Latin hypercube sampling is employed to generate uniformly distributed initial samples, and the Kriging regression function and correlation function are set to the zero-order polynomial and Gaussian function, respectively. Moreover, the hyperparameter optimization range for Kriging modeling in all methods is set to $[0, 9]$.

$$error = \frac{|P_F - P_{Fmc}|}{P_{Fmc}} \times 100\% \quad (29)$$

where, P_{Fmc} is the failure probability estimated using the MC method; P_F is the failure probability predicted using compared approaches. The $error$ formula used cannot handle the issue of $P_{Fmc} = 0$.

4.1. Case I: a mathematical example

The first example is a mathematical model 53, its time-variant limit state function (TLSF) is described as:

$$g(X_1, X_2, Y(t), t) = X_1^2 X_2 - 5X_1(1 + Y(t))t + (X_2 + 1)t^2 - 20(30)$$

where, t is the time parameter varying from 0 to 1; X_1 and X_2 are two independent random variables; $Y(t)$ is a Gaussian stochastic process. Their distribution features are showed in

Table 1. Random parameters for case I.

Variable	Distribution	Mean	Standard deviation	Autocorrelation function
X_1	Normal	3.5	0.25	/
X_2	Normal	3.5	0.25	/
$Y(t)$	Gaussian process	0	1	$\rho_{Y(t_1, t_2)} = \exp(-(t_2 - t_1)^2)$

Given the eigenvalue situation, the stochastic process is expanded into three random variables using the EOLE method, and the time interval is discretized into 50 time nodes.

presents the calculation results of different methods, it can be observed that the proposed RSTK can acquire satisfactory computing precision. Figure 10 illustrates the iterative process of reliability-sensitive segments of 200 candidate trajectories; the number of reliability-sensitive segments requiring iterative computation decreases significantly as the iteration progresses. Notably, the proposed RSTK holds the lowest CPU computing time, and it is one order of magnitude less than that of eSPT, SILK, REAL, and SSTK, which displays the significant superiority of the RSTK method in reducing iterative computing

time. This is because non-reliability-sensitive space-time data are adaptively excluded during RSTK-based iterations, effectively avoiding a large number of redundant and ineffective calculations in the candidate pool. Moreover, the N_{call} required by RSTK is the least, demonstrating the superiority of the RSTK method in reducing surrogate modeling cost. The convergence metrics for different methods are as follows: $CCL = 99.9993\%$, $MPE = 1.35\%$, $MREE = 3.95\%$, $U_x = 2.72$, $IAU = 3.71$, and $(C = 98.48\%$ and $er_{\text{max}} = 3.61\%$).

Table 2. Average result of 20 runs for case I.

Method	N_{call}	P_f	Relative error (%)	Computing time, s
MC	$10^6 \times 50$	0.3081	/	0.43
eSPT	56.3	0.3081	0	4114.5
SILK	22.1	0.3064	0.55	1412.2
REAL	22.0	0.3006	2.43	1375.1
SLK-CSPR	48.5	0.3087	0.19	224.5
SSTK	41.2	0.3091	0.32	4939.1
RSTK	20.6	0.3037	1.43	169.1

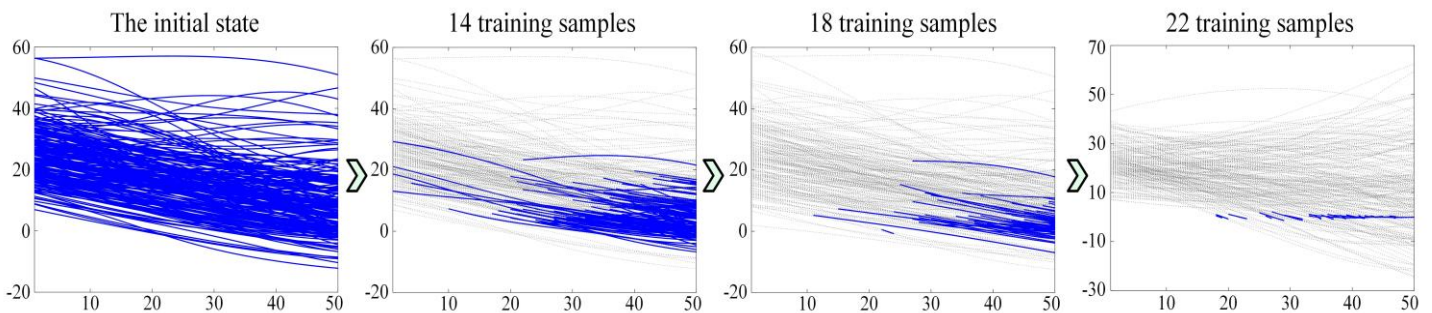


Figure 10. Variation process of the reliability-sensitive segment (i.e., the blue segment) for Case I.

4.2. Case II: a corroded simply supported beam

A simply supported beam commonly used in civil engineering is adopted as the second case 54, as depicted in Figure 11. The

random input vector $X = [f_y, b_0, h_0, F(t)]$, where f_y is the ultimate stress, b_0 is the initial width, h_0 is the initial height, and $F(t)$ is the dynamic load. Their distribution characteristics are shown in

. The structure is subjected to a static force $p = 78500 h_0 b_0$ (N/m) and its length $L = 5$ m. Moreover, b_0 and h_0 decrease over time due to corrosion, as described below:

$$b(t) = b_0 - 2kt; h(t) = h_0 - 2kt \quad (31)$$

where, $k = 0.05$ mm/year is the corrosion coefficient, and $t \in [0,$

10]. The structure fails when the maximum bending moment exceeds the ultimate bending moment. The TLSF is then formulated as follows:

$$g(f_y, b_0, h_0, F(t), t) = \frac{b(t)h(t)^2 f_y}{4} - \frac{F(t)L}{4} - \frac{78500 b_0 h_0 L^2}{8} \quad (32)$$

Table 3. Random parameters for case II.

Variable	Distribution	Mean	Standard deviation	Autocorrelation function
b_0	Lognormal	0.2 m	0.01 m	/
h_0	Lognormal	0.04 m	0.004 m	/
f_y	Lognormal	240 MPa	24 MPa	/
$F(t)$	Gaussian process	6500 N	650 N	$\rho_{F(t)}(t_1, t_2) = \exp(-144(t_1 - t_2)^2)$

The stochastic process is expanded into 30 random variables using the EOLE method, and the time interval is discretized into 300 time nodes. Figure 12 shows the iterative process of reliability-sensitive segments.

lists the computing results of different methods. The results indicate that the RSTK can obtain satisfactory calculation accuracy, with its failure probability (0.0135) closely matching the reference value (0.0137) obtained by MC. In addition, the N_{call} required by the proposed RSTK is close to that of REAL and lower than those of all other comparison methods. The CPU computing time required by RSTK is only 5% of that of REAL, while RSTK achieves similar computational accuracy and

surrogate cost as REAL. Furthermore, the CPU computing time required by RSTK is the shortest, being two orders of magnitude lower than that of eSPT, SILK, REAL, and SSTK, which illustrates the significant superiority of the proposed method in iterative computation efficiency. The convergence metrics for different methods are as follows: $CCL = 99.9991\%$, $MPE = 4.03\%$, $MREE = 2.98\%$, $Ux = 2.21$, $IAU = 3.22$, and $(C = 99.92\%$ and $er_{\text{max}} = 4.71\%)$.

Table 4. Average result of 20 runs for case II.

Method	N_{call}	P_f	Relative error (%)	Computing time, s
MC	$10^6 \times 300$	0.0137	/	3.82
eSPT	44.3	0.0137	0	17217.7
SILK	25.2	0.0138	0.73	11894.7
REAL	23.5	0.0139	1.46	10204.9
SLK-CSPR	35.7	0.0138	0.73	767.8
SSTK	31.4	0.0138	0.73	17381.5
RSTK	23.7	0.0135	1.46	535.1

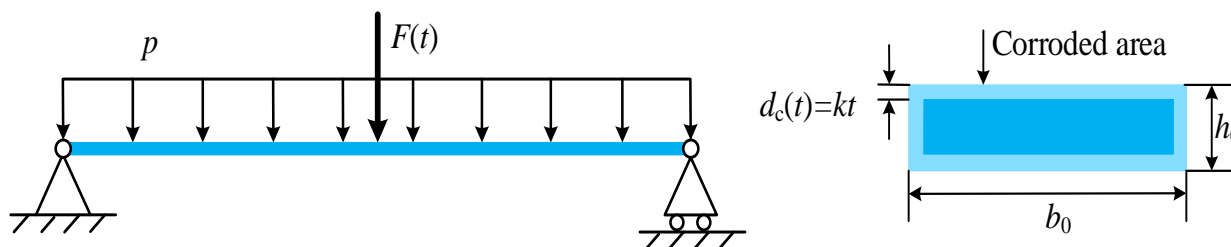


Figure 11. Corroded simple supported beam.

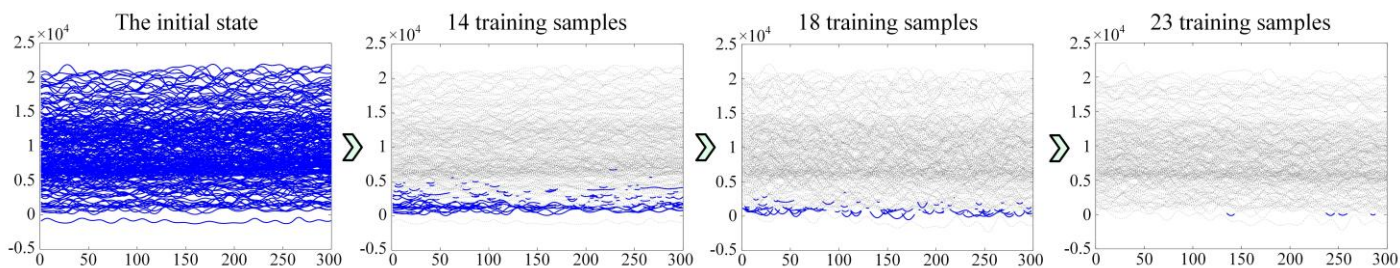


Figure 12. Variation process of the reliability-sensitive segment for Case II

4.3. Case III: a roof truss structure

A roof truss is studied 55, as shown in Figure 13, in which the nodal load $P = q(t)l/4$ and $q(t)$ represents a dynamic uniform load. The truss will fail when the perpendicular deflection of the node C exceeds the allowable value 0.03, and the TLSF is formulated as follows:

$$g(l, A_c, E_c, A_s, E_s, q(t), t) = 0.03 - \frac{q(t)l^2}{2} \left(\frac{3.81}{A_c E_c} + \frac{1.13}{A_s E_s} \right) \quad (33)$$

where, t is the time parameter varying from 0 to 1; l is the structure length; A_c and A_s are the cross-sectional areas of reinforced concrete and steel bars, respectively, and E_c and E_s are their corresponding elastic modulus. The distributed characteristics of random inputs are shown in Table 5.

The stochastic process is expanded into 10 random variables using the EOLE method, and the time interval is discretized into

50 time nodes. Figure 14 displays the iterative process of reliability-sensitive segments. It can be seen from Table 6 that the proposed method can obtain satisfactory accuracy. The N_{call} required by RSTK is significantly lower than that of the comparison methods. Specifically, RSTK requires 50.6 N_{call} , which is 22.3% less than the 65.1 N_{call} required by REAL, the best-performing method among the comparisons. This demonstrates the significant advantage of the proposed method in reducing the cost of actual response evaluation. Moreover, in terms of CPU computing time, the proposed method is two orders of magnitude faster than SILK and SSTK, and one order of magnitude faster than eSPT and REAL, which reflects its remarkable superiority in decreasing iterative computation time. The convergence metrics for different methods are as follows: $CCL = 99.9991\%$, $MPE = 4.76\%$, $MREE = 4.34\%$, $U_x = 2.01$, $IAU = 4.24$, and ($C = 99.76\%$ and $er_{\text{max}} = 4.41\%$).

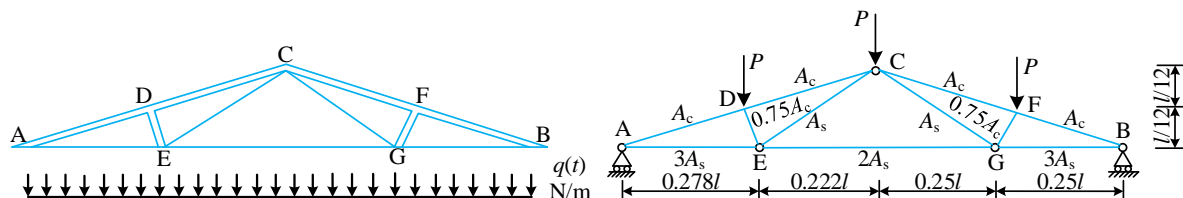


Figure 13. Roof truss structure .

Table 5. Random parameters for case III.

Variable	Distribution	Mean	Standard deviation	Autocorrelation function
l	Normal	12	0.12	/
A_c	Normal	0.04	0.0048	/
E_c	Normal	2×10^{10}	1.2×10^9	/
A_s	Normal	9.82×10^{-4}	5.982×10^{-5}	/
E_s	Normal	1×10^{11}	6×10^9	/
$q(t)$	Gaussian process	2×10^4	1.4×10^3 N	$\rho_{q(t_1, t_2)} = \exp(-9(t_1 - t_2)^2)$

Table 6. Average result of 20 runs for case III.

Method	N_{call}	P_f	Relative error (%)	Computing time, s
MC	$10^6 \times 50$	0.0336	/	0.49
eSPT	128.3	0.0336	0	9181.8
SILK	84.2	0.0335	0.3	10105.9
REAL	65.1	0.0331	1.49	6209.2

SLK-CSPR	117.3	0.0325	3.27	201.3
SSTK	101.6	0.0330	1.79	12009.9
RSTK	50.6	0.0331	1.49	153.9

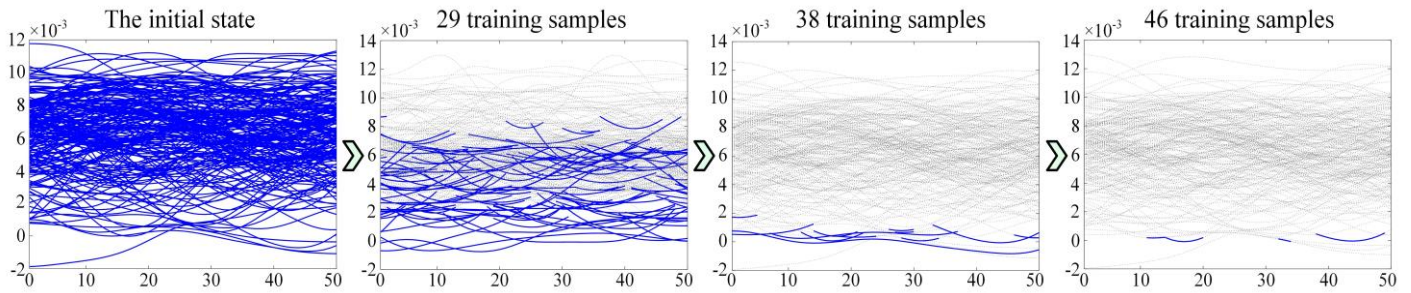


Figure 14. Variation process of the reliability-sensitive segment for Case III .

4.4. Case IV: a self-balancing vehicle

The self-balancing vehicle 42, widely used in daily life is employed as the engineering case. It consists of a lighting module, driving wheel, control unit, and chassis, as shown in Figure 15. The chassis must withstand dynamic loads under various working conditions, such as cornering, deceleration, and acceleration. In this study, the most common loading condition is considered, in which the chassis is subjected to two equal time-variant random loads $Y(t)$ at symmetrical locations, as shown in Figure 16. To guarantee driving stability, the deformation of the chassis should be less than the allowable threshold 42,, and the TLSF is described as follows:

$$g(D_{\text{allow}}(t_0), X_1, X_2, E, Y(t), t) = [D_{\text{allow}}] - D(X_1, X_2, E, Y(t), t) \quad (34)$$

where, X_1 and X_2 are the chassis length and chassis width, respectively; E is the material elastic modulus; $[D_{\text{allow}}] = D_{\text{allow}}(t_0) \cdot \exp(-0.002t)$ is the allowable deformation, and it will decrease within time $t \in [0, 48]$ months; $D_{\text{allow}}(t_0)$ is the initial

allowable deformation. The statistical characteristics of variables are listed in Table 7.

The stochastic process is expanded into 100 random variables using the EOLE method, and the time interval is discretized into 200 time nodes. Figure 17 illustrates the iterative process of reliability-sensitive segments. Table 8 presents the calculating results of various approaches. It can be seen that the failure assessment results obtained using the RSTK are similar to the results of other comparison methods, which demonstrates the effectiveness of the proposed method in the engineering case. Moreover, the N_{call} required by RSTK is lower than all methods except REAL, and the CPU computing time required using RSTK is the lowest, being one order of magnitude less than that of eSPT, SILK, REAL, and SSTK. This reflects the superiority of the proposed approach in reducing computing cost. The convergence metrics for different methods are as follows: $CCL = 99.9992\%$, $MPE = 4.84\%$, $MREE = 2.45\%$, $U_x = 2.21$, $IAU = 3.16$, and $(C = 99.64\%$ and $er_{\text{max}} = 3.84\%)$.

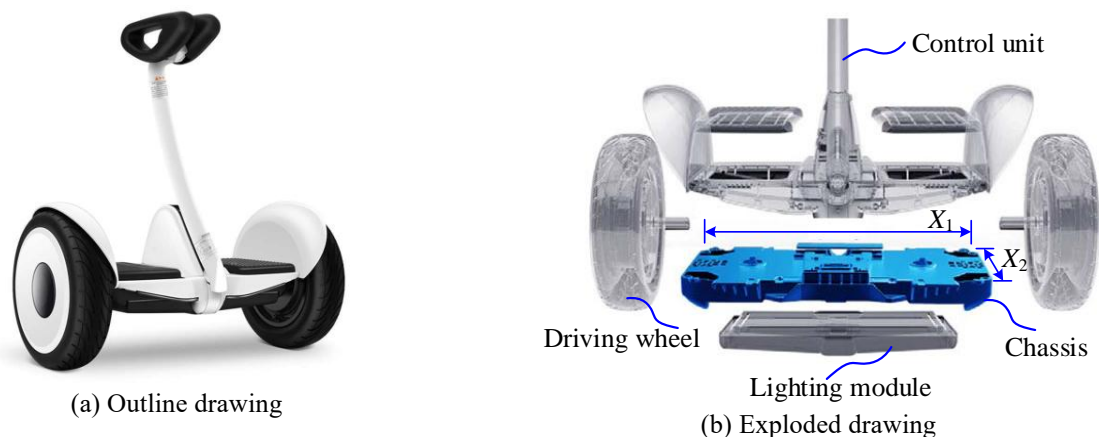


Figure 15. Self-balancing vehicle.

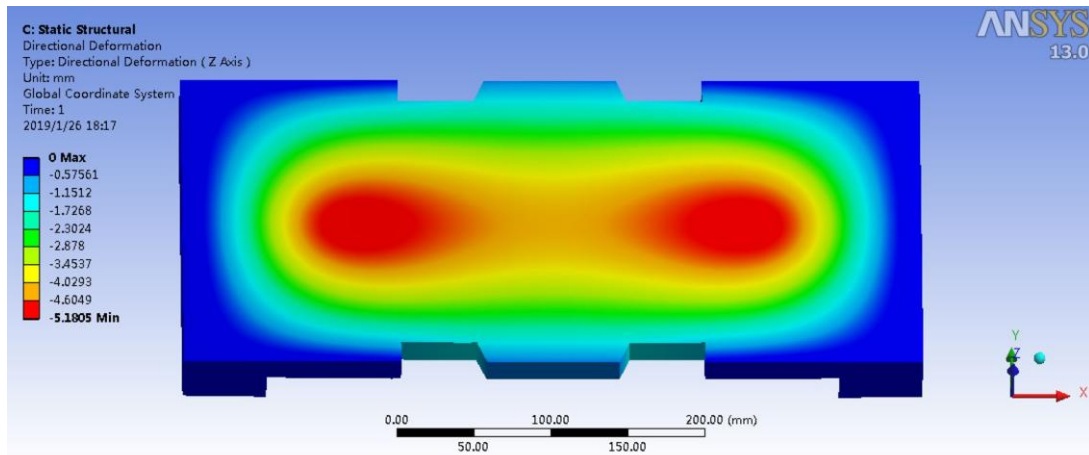


Figure 16. Finite element simulation of chassis.

Table 7. Random parameters for case IV.

Variable	Distribution	Mean	Standard deviation	Autocorrelation function
X_1 (mm)	Lognormal	480	4.8	/
X_2 (mm)	Lognormal	220	2.2	/
E (MPa)	Lognormal	72000	2000	/
$D_{allow}(t_0)$ (mm)	Normal	5	0.1	/
$Y(t)$ (MPa)	Gaussian process	1.5	0.1	$\rho_{Yt}(t_1, t_2) = \exp(-10(t_1-t_2)^2)$

Table 8. Average result of 10 runs for case IV.

Method	N_{call}	P_f	Computing time, s
eSPT	95.7	0.0422	36019.9
SILK	82.3	0.0422	49021.3
REAL	56.3	0.0412	25977.4
SLK-CSPR	109.5	0.0419	1379.1
SSTK	96.7	0.0421	87502.4
RSTK	65.5	0.0419	1102.4

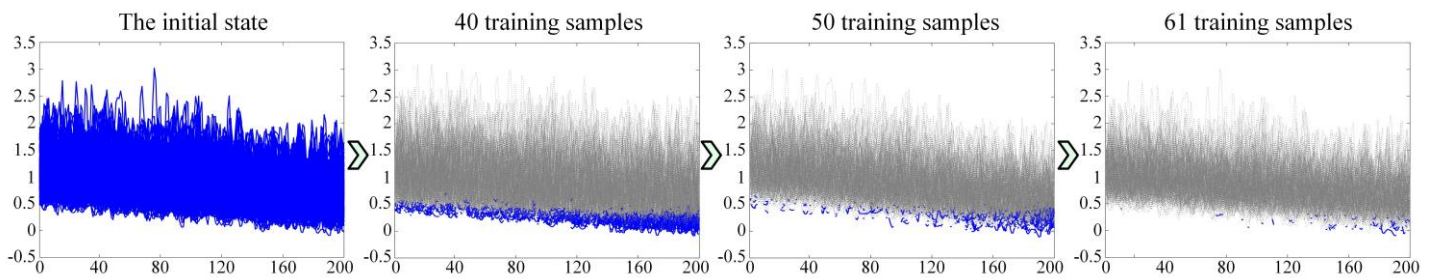


Figure 17. Variation process of the reliability-sensitive segment for Case IV.

It can be observed from the above case analysis that the proposed method not only reduces the surrogate cost but also minimizes the CPU calculation time, all while maintaining calculation accuracy. This can be attributed to the fact that RSTK fully focuses on reliability-sensitive space-time regions during adaptive sample screening and iterative calculations. This verifies the positive impact of the adaptive learning design, which excludes low-quality candidate data, on ensuring the efficacy of TRA.

5. Conclusions and outlooks

This study firstly proposes the concept of fully focusing on reliability-sensitive space-time and designs the corresponding adaptive surrogate modeling method. The main contribution of this study is that it first proposes the concept of adaptive time-variant surrogate modeling that fully focuses on reliability-sensitive space-time, and elucidates its importance in ensuring the efficacy of time-variant reliability analysis. The computational superiority demonstrated by the proposed RSTK reveals the importance of sufficiently concentrating surrogate learning on the reliability-sensitive space-time region to elevate

the efficacy of time-variant reliability analysis. Two aims are achieved using the proposed RSTK. First, the surrogate modeling cost is reduced by selectively capturing high-quality reliability-sensitive data. Second, the iterative calculation time is reduced by removing enormous non-reliability-sensitive trajectory segments during the iterative estimation process. Four case studies are analyzed, and the conclusions are drawn based on the results, as follows:

(1) The adaptive operation, which concentrates surrogate learning on the reliability-sensitive space-time region, facilitates capturing high-quality reliability-promoting surrogate samples, as it effectively avoids focusing on the low-return sub-regions where accurate reliability judgments have been achieved.

(2) There are considerable non-reliability-sensitive trajectory segments in the time-variant candidate pool that perform poorly in promoting adaptive surrogate modeling.

Acknowledgments

This paper is co-supported by the National Natural Science Foundation of China (No. 52205164 and 52405145), the Research Start-up Funds of Hangzhou International Innovation Institute of Beihang University (No. 2024KQ085), and the Insight Action (No. F5C15B07). The authors would like to thank them.

References

1. Gao H F, Wang Y H, Li Y, Zio E. Distributed-collaborative surrogate modeling approach for creep-fatigue reliability assessment of turbine blades considering multi-source uncertainty. *Reliability Engineering & System Safety*, 2024, 250: 110316. <http://doi.org/10.1016/j.res.2024.110316>.
2. Chen Pe Y, Zhao C B, Yao H, Zhao S N. An adaptive method based on PC-Kriging for system reliability analysis of truss structures. *Eksploatacja i Niezawodność - Maintenance and Reliability*, 2023, 25(3): 169497. <http://doi.org/10.17531/ein/169497>.
3. Fei C Wei, Han Y J, Wen J R, Li C, Han L, Choyb Y S. Deep learning-based modeling method for probabilistic LCF life prediction of turbine blisk. *Propulsion and Power Research*, 2024, 13(1): 12-25. <https://doi.org/10.1016/j.jprr.2023.08.005>.
4. Fei C W, Li H, Liu H T, Lu C, An L Q, Han L, Zhao Y J. Enhanced network learning model with intelligent operator for the motion reliability evaluation of flexible mechanism. *Aerospace Science and Technology*, 2020, 107: 106342. <https://doi.org/10.1016/j.ast.2020.106342>.
5. Lu C, Teng D, Chen J Y, Fei C W, Keshtegar B. Adaptive vectorial surrogate modeling framework for multi-objective reliability estimation. *Reliability Engineering and System Safety*, 2023, 234: 109148. <https://doi.org/10.1016/j.res.2023.109148>.
6. Fei C W, Li H, Liu H T, Lu C, Keshtegar B, An L Q. Multilevel nested reliability-based design optimization with hybrid intelligent regression for operating assembly relationship. *Aerospace Science and Technology*, 2020, 103: 105906. <https://doi.org/10.1016/j.ast.2020.105906>.
7. Fei C W, Li C, Lin J Y, Han Y J, Choy Y S, Chen C H. Structural design of aeroengine radiators: State of the art and perspectives. *Propulsion and Power Research*, 2024, 13(3): 319-334. <https://doi.org/10.1016/j.jprr.2024.08.004>.
8. Meng Z, Zhang D Q, Li G, Yu B. An importance learning method for non-probabilistic reliability analysis and optimization. *Structural and Multidisciplinary Optimization*, 2019, 59: 1255-1271. <https://doi.org/10.1007/s00158-018-2128-7>.
9. Meng Z, Zhang Z H, Zhang D Q, Yang D X. An active learning method combining Kriging and accelerated chaotic single loop approach

Removing these trajectory segments during the iterative calculation can reduce the TRA iteration time by orders of magnitude.

(3) The case study reveals that the proposed RSTK can obtain satisfactory computational accuracy by using lower surrogate cost and calculating time.

Although this study provides a feasible and efficient time-variant reliability analysis approach, the limitation does exist. In small failure issues, it is challenging for the proposed method to capture high-quality training data since the candidate data near the limit state are scarce. Moreover, based on the surrogate modeling concept of adequately focusing on the reliability-sensitive region, designing other, more effective learning mechanisms is a work worth exploring. Extending the proposed reliability-sensitive focusing concept to time-variant system reliability problems is a direction worth investigating. Future work will further explore these issues.

- (AK-ACSLA) for reliability-based design optimization. *Computer Methods in Applied Mechanics and Engineering*, 2019, 357: 112570. <https://doi.org/10.1016/j.cma.2019.112570>.
10. Meng Z, Kong L, Yi J X, Peng H. Optimum-pursuing method for constrained optimization and reliability-based design optimization problems using Kriging model. *Computer Methods in Applied Mechanics and Engineering*, 2024, 420: 116704. <https://doi.org/10.1016/j.cma.2023.116704>.
 11. Kubica J, Ahmed B, Muhammad A, Aslam M U. Dynamic reliability calculation of random structures by conditional probability method. *Eksploatacja i Niezawodność - Maintenance and Reliability*, 2024, 26(2): 181133. <http://doi.org/10.17531/ein/181133>.
 12. Li Y, Gao H F, Chen H T, Liu C, Yang Z, Zio E. Accelerated degradation testing for lifetime analysis considering random effects and the influence of stress and measurement errors. *Reliability Engineering and System Safety*, 2024, 247: 110101. <http://doi.org/10.1016/j.res.2024.110101>.
 13. Wang D P, Jiang C, Qiu H B, Zhang J H, Gao L. Time-dependent reliability analysis through projection outline-based adaptive Kriging. *Structural and Multidisciplinary Optimization*, 2020, 61(4): 1453-1472. <http://doi.org/10.1007/s00158-019-02426-0>.
 14. Reffas O, Sahraoui Y, Nahal M, Ghoul R H, Saad S. Reactive energy compensator effect on the reliability of a complex electrical system using Bayesian networks. *Eksploatacja i Niezawodność - Maintenance and Reliability*, 2020, 22(4): 684-693. <http://doi.org/10.17531/ein.2020.4.12>.
 15. Jiang C, Ni B Y, Han X, Tao Y R. Non-probabilistic convex model process: A new method of time-variant uncertainty analysis and its application to structural dynamic reliability problems. *Computer Methods in Applied Mechanics and Engineering*, 2014, 268: 656-676. <http://doi.org/10.1016/j.cma.2013.10.016>.
 16. Ling C Y, Lu Z Z. Adaptive Kriging coupled with importance sampling strategies for time-variant hybrid reliability analysis. *Applied Mathematical Modelling*, 2020, 77: 1820-1841. <http://doi.org/10.1016/j.apm.2019.08.025>.
 17. Rice S O. Mathematical analysis of random noise. *The Bell System Technical Journal*, 1945, 24(1): 46-156. <https://doi.org/10.1002/j.1538-7305.1945.tb00453.x>.
 18. Andrieu-Renaud C, Sudret B, Lemaire M. The PHI2 method: A way to compute time-variant reliability. *Reliability Engineering & System Safety*, 2004, 84(1): 75-86. <http://doi.org/10.1016/j.res.2003.10.005>.
 19. Sudret B. Analytical derivation of the outcrossing rate in time-variant reliability problems. *Structure and Infrastructure Engineering*, 2008, 4(5): 353-362. <http://doi.org/10.1080/15732470701270058>.
 20. Hu Z, Du X. Time-dependent reliability analysis with joint upcrossing rates. *Structural and Multidisciplinary Optimization*, 2013, 48(5): 893-907. <http://doi.org/10.1007/s00158-013-0937-2>.
 21. Jiang C, Wei X P, Huang Z L, Liu J. An outcrossing rate model and its efficient calculation for time-dependent system reliability analysis. *Journal of Mechanical Design*, 2017, 139: 041402. <http://doi.org/10.1115/1.4035792>.
 22. Yu S, Zhang Y, Li Y, Wang Z. Time-variant reliability analysis via approximation of the first-crossing PDF. *Structural and Multidisciplinary Optimization*, 2020, 62(5): 2653-2667. <http://doi.org/10.1007/s00158-020-02635-y>.
 23. Jiang C, Huang X P, Han X, Zhang D Q. A time-variant reliability analysis method based on stochastic process discretization. *Journal of Mechanical Design*, 2014, 136: 091009. <http://doi.org/10.1115/1.4027865>.
 24. Jiang C, Wei X P, Wu B, Huang Z L. An improved TRPD method for time-variant reliability analysis. *Structural and Multidisciplinary Optimization*, 2018, 58(5): 1935-1946. <http://doi.org/10.1007/s00158-018-2002-7>.
 25. Gong C, Frangopol D M. An efficient time-dependent reliability method. *Structural Safety*, 2019, 81: 101864. <http://doi.org/10.1016/j.strusafe.2019.05.001>.
 26. Meng Z, Zhao J Y, Jiang C. An efficient semi-analytical extreme value method for time-variant reliability analysis. *Structural and Multidisciplinary Optimization*, 2021, 64: 1469-1480. <https://doi.org/10.1007/s00158-021-02934-y>.
 27. Li F Y, Liu J, Yan Y F, Rong J H, Yi J J. A time-variant reliability analysis method based on the stochastic process discretization under random and interval variables. *Symmetry-basel*, 2021, 13(4): 568. <http://doi.org/10.3390/sym13040568>.
 28. Yao Q S, Zhang Q, Tang J C, Wang X P, Hu M J. Time-variant reliability analysis method for uncertain motion mechanisms based on stochastic process discretization. *IEEE ACCESS*, 2022, 10: 49040-49049. <http://doi.org/10.1109/ACCESS.2022.3153524>.
 29. Huang Y, Zhang J G, Wang B W, Song L K, Gong Q, Wei Y. AOK-ES: Adaptive optimized Kriging combining efficient sampling for

- structural reliability analysis. *Quality and Reliability Engineering International*, 2024, 40(4): 1502-1525. <http://doi.org/10.1002/qre.3493>.
30. Huang Y, Zhang J G, Fan X D, Gong Q, Song L K. A novel reliability analysis method for engineering problems: Expanded learning intelligent back propagation neural network. *Chinese Journal of Aeronautics*, 2024, 37(12): 212-230. <http://doi.org/10.1016/j.cja.2024.05.044>.
 31. Li C, Wen J R, Wan J, Taylan O, Fei C W. Adaptive directed support vector machine method for the reliability evaluation of aeroengine structure. *Reliability engineering & system safety*, 2024, 246: 110064. <http://doi.org/10.1016/j.res.2024.110064>.
 32. Gao H F, Zio E, Guo J J, Bai G C, Fei C W. Dynamic probabilistic-based LCF damage assessment of turbine blades regarding time-varying multi-physical field loads. *Engineering Failure Analysis*, 2020, 108: 104193. <https://doi.org/10.1016/j.engfailanal.2019.104193>.
 33. Fei C W, Tang W Z, Bai G C. Novel method and model for dynamic reliability optimal design of turbine blade deformation. *Aerospace Science and Technology*, 2015, 39: 588-595. <https://doi.org/10.1016/j.ast.2014.07.003>.
 34. Lu C, Fei C W, Feng Y W, Zhao Y J, Dong X W, Choy Y S. Probabilistic analyses of structural dynamic response with modified Kriging-based moving extremum framework. *Engineering Failure Analysis*, 2021, 12: 105398. <https://doi.org/10.1016/j.engfailanal.2021.105398>.
 35. Wang D P, Qiu H B, Gao L, Jiang C. A subdomain uncertainty-guided kriging method with optimized feasibility metric for time-dependent reliability analysis. *Reliability Engineering & System Safety*, 2023, 243: 109839. <http://doi.org/10.1016/j.res.2023.109839>.
 36. Wang D P, Qiu H B, Gao L, Xu, D Y, Jiang C. Time-dependent system reliability analysis using adaptive single-loop Kriging with probability of rejecting classification. *Structural and Multidisciplinary Optimization*, 2023, 66(8): 186. <http://doi.org/10.1007/s00158-023-03638-1>.
 37. Wang Z, Wang P. A nested extreme response surface approach for time-dependent reliability-based design optimization. *Journal of Mechanical Design*, 2012, 134(12): 121007. <http://doi.org/10.1115/1.4007931>.
 38. Hu Z, Du X. Mixed efficient global optimization for time-dependent reliability analysis. *Journal of Mechanical Design*, 2015, 137(5): 051401. <http://doi.org/10.1115/1.4029520>.
 39. Wang Z, Chen W. Time-variant reliability assessment through equivalent stochastic process transformation. *Reliability Engineering & System Safety*, 2016, 152: 166-175. <http://doi.org/10.1016/j.res.2016.02.008>.
 40. Hu Z, Mahadevan S. A single-loop Kriging surrogate modeling for time-dependent reliability analysis. *Journal of Mechanical Design*, 2016, 138: 061406. <http://doi.org/10.1115/1.4033428>.
 41. Echard B, Gayton N, Lemaire M. AK-MCS: An active learning reliability method combining Kriging and Monte Carlo simulation. *Structural Safety*, 2011, 33: 145-154. <http://doi.org/10.1016/j.strusafe.2011.01.002>.
 42. Jiang C, Qiu H B, Gao L, Wang D P, Yang Z, Chen Li M. Real-time estimation error-guided active learning Kriging method for time-dependent reliability analysis. *Applied Mathematical Modelling*, 2020, 77: 82-98. <http://doi.org/10.1016/j.apm.2019.06.035>.
 43. Gao L X, Lu Z Z, Feng K X, Hu Y S, Jiang X. Advanced surrogate-based time-dependent reliability analysis method by an effective strategy of reducing the candidate sample pool. *Structural and Multidisciplinary Optimization*, 2021, 64(4): 2199-2212. <http://doi.org/10.1007/s00158-021-02975-3>.
 44. Tian Z R, Zhi P P, Guan Y, Feng J B, Zhao Y D. An effective single loop Kriging surrogate method combining sequential stratified sampling for structural time-dependent reliability analysis. *Structures*, 2023, 53: 1215-1224. <http://doi.org/10.1007/s00158-021-02975-3>.
 45. Jiang C, Qiu H B, Yang Z, Chen L M, Gao L, Li P G. A general failure-pursuing sampling framework for surrogate-based reliability analysis. *Reliability Engineering & System Safety*, 2019, 183: 47-59. <http://doi.org/10.1016/j.res.2018.11.002>.
 46. Jiang C, Wang D P, Qiu H B, Gao L, Chen L M, Yang Z. An active failure-pursuing Kriging modeling method for time-dependent reliability analysis. *Mechanical Systems and Signal Processing*, 2019, 129: 112-129. <http://doi.org/10.1016/j.ymsp.2019.04.034>.
 47. Wang D P, Qiu H B, Gao L, Jiang C. A single-loop Kriging coupled with subset simulation for time-dependent reliability analysis. *Reliability Engineering & System Safety*, 2021, 216: 107931. <http://doi.org/10.1016/j.res.2021.107931>.
 48. Song Z, Zhang H, Zhang L, Liu Z, Zhu P. An estimation variance reduction-guided adaptive Kriging method for efficient time-variant structural reliability analysis. *Mechanical Systems and Signal Processing*, 2022, 178: 109322. <http://doi.org/10.1016/j.ymsp.2022.109322>.
 49. Li C C, Der Kiureghian A. Optimal discretization of random fields. *Journal of Mechanical Design*, 1993, 119(6): 1136-1154. [https://doi.org/10.1061/\(ASCE\)0733-9399\(1993\)119:6\(1136\)](https://doi.org/10.1061/(ASCE)0733-9399(1993)119:6(1136)).
 50. Nan H, Li H S, Song Z C. An adaptive PC-Kriging method for time-variant structural reliability analysis. *Eksplotacja i Niezawodność -*

- Maintenance and Reliability, 2022, 24 (3): 532-543. <http://doi.org/10.17531/ein.2022.3.14>.
51. Huang Y, Zhang J G, Song L K, Li X Q, Bai G C. A unified reliability evaluation framework for aircraft turbine rotor considering multi-site failure correlation. *Structural and Multidisciplinary Optimization*, 2023, 66: 171. <http://doi.org/10.1007/s00158-023-03628-3>.
 52. Qian H M, Huang H Z, Li Y F. A novel single-loop procedure for time-variant reliability analysis based on Kriging model. *Applied Mathematical Modelling*, 2019, 75: 735-748. <http://doi.org/10.1016/j.apm.2019.07.006>.
 53. Zhang D Q, Zhou P F, Jiang C, Yang M D, Han X, Li Q. A stochastic process discretization method combing active learning Kriging model for efficient time-variant reliability analysis. *Computer Methods in Applied Mechanics and Engineering*, 2021, 384: 113990. <http://doi.org/10.1016/j.cma.2021.113990>.
 54. Hu Y S, Lu Z Z, Wei N, Jiang X, Zhou C C. Advanced single-loop Kriging surrogate model method by combining the adaptive reduction of candidate sample pool for safety lifetime analysis. *Applied Mathematical Modelling*, 2021, 100: 580-595. <http://doi.org/10.1016/j.apm.2021.08.019>.
 55. Ji Y X, Liu H, Xiao N C, Zhan H Y. An efficient method for time-dependent reliability problems with high-dimensional outputs based on adaptive dimension reduction strategy and surrogate model. *Engineering Structures*, 2023, 276: 115393. <http://doi.org/10.1016/j.engstruct.2022.115393>.
 56. Huang Z L, Jiang C, Li X M, Wei X P, Fang T, Han X. A single-loop approach for time-variant reliability-based design optimization. *IEEE Transaction on Reliability*, 2017, 66: 651-661. <http://doi.org/10.1109/TR.2017.2703593>.